

The cross-sectional warping problem for hyperelastic beams: An efficient formulation in Voigt notation

Juan C. Alzate Cobo^{1*}, Tobias Henkels¹ and Oliver Weeger¹

¹Cyber-Physical Simulation, Technical University of Darmstadt, Dolivostr. 15,
Darmstadt, 64293, Germany.

*Corresponding author(s). E-mail(s): alzate@cps.tu-darmstadt.de;

Abstract

Beam theory has traditionally been restricted to small elastic strains and rigid cross-sections. Relaxing these assumptions within closed-form analytical frameworks remains challenging. In contrast, the cross-sectional warping problem provides a computational approach that enables the derivation of general, nonlinear constitutive relations for beam models, thereby overcoming both limitations. In this work, we reinterpret the cross-sectional warping problem for hyperelastic beams and propose a fully material formulation in terms of the Green-Lagrange strain and the second Piola-Kirchhoff stress tensors. Owing to the symmetry of these tensors, the formulation can be expressed efficiently in Voigt notation and is thus particularly well-suited for straightforward numerical implementation. We demonstrate the validity of this alternative formulation in numerical examples, including the computation of the effective beam stiffness, for which we derive the sensitivities of the warping displacement. To promote reproducibility, we accompany this article with an open-access repository containing the isogeometric finite element implementation and all numerical examples presented herein, enabling other researchers to readily reproduce and build upon our results.

Keywords: Beam theory, Nonlinear constitutive relations, Cross-sectional warping, Voigt notation, Isogeometric analysis

1 Introduction

Beam-based structures are widely used in applications involving nonlinear and inelastic material behavior, including concrete reinforcements, soft robots, mechanical and multiphysical metamaterials, woven and knitted textiles, and more [1–9]. However, the computational design and simulation of such structures using three-dimensional (3D) continuum models and their finite element discretizations are computationally intensive, and more efficient alternatives are therefore desirable. One such alternative is provided by one-dimensional (1D) models based on beam theory.

Nevertheless, classical beam theory exhibits major limitations: it is restricted to small strains, linear elastic material behavior, and deformations in which the cross-section remains planar [10–14].

Enhancing beam theory with nonlinear constitutive models is far from trivial. Recently, significant research has been made to extend classical beam theory to include finite elastic strains and hyperelastic materials [15, 16], plasticity and visco-elasticity at small strains [17–20], chemo-elasticity [21], and even large swelling expansions caused by anisotropic diffusion [22]. However, the aforementioned works are either based on additional degrees of freedom, on small elastic strains,

on overly restrictive kinematics, or are even incomplete, as can be seen in the context of plasticity, for which yield surfaces and hardening laws in terms of stress resultants, i.e., in terms of forces and moments, are still a matter of active investigation [23–25]. Most importantly, a unifying approach for obtaining beam constitutive models which includes hyperelastic materials, inelastic effects such as swelling and visco-elasto-plasticity at both large and small strains, and that is simultaneously conformal with 3D continuum kinematics, i.e., that allows cross-sectional deformations, is largely missing from the literature.

In order to bridge the gap between computationally efficient yet kinematically restricted beam models and their kinematically general but numerically expensive 3D continuum counterparts, Arora et al. [26] introduced the cross-sectional warping problem (CSWP). The CSWP is based on the Helical Cauchy-Born rule (HCB) proposed by Kumar et al. [27], which reduces beam deformations to a family of helical configurations by imposing a uniform strain field along the beam centerline. These configurations depend solely on the six strain measures of beam theory. Owing to the uniformity of the strain field along the beam axis, the problem reduces to the cross-section and can be formulated as a boundary value problem (BVP). Its solution yields cross-sectional deformations, from which resultant forces, moments, and stiffnesses can be obtained for arbitrary strain states. By modeling the cross-section as a two-dimensional (2D) continuum with three displacement degrees of freedom, the CSWP captures both in-plane and out-of-plane deformations and accommodates general hyperelastic material behavior. Typically, the resulting BVP is discretized and solved using an isoparametric finite element formulation [26].

In recent years, the CSWP and variations thereof have been used for the determination of a variety of nonlinear beam constitutive relations and cross-sectional effects. For example, Singh et al. [28] enhanced it with surface energy, Herrnböck et al. [23] employed it for obtaining yield surfaces in terms of beam measures and then enhanced the model to include hardening [24], Vinayak et al. [29] used it for modeling anisotropic plasticity, Kumar et al. [30] used it as a foundation for obtaining nonlinear elastic constitutive models in strips, and, most recently, Kumar et al.

[31] extended it to include cross-sectional growth. Additionally, the CSWP has been embedded in FE²-type concurrent multiscale frameworks in elasto-plastic beams with hardening [24, 32] and for hyperelastic, shear-rigid beams [33], where it replaces an explicit constitutive model. Furthermore, it has been used for data generation in the context of learning hyperelastic beam constitutive models using thermodynamically consistent neural networks [34, 35].

One drawback of the CSWP formulation proposed by Arora et al. [26], and its subsequent extensions [23, 24, 28, 29, 31], lies in its energy-conjugate formulation in terms of the first Piola-Kirchhoff (PK1) stress tensor and the deformation gradient. In particular, its numerical implementation requires the manipulation of full, non-symmetric second-order stress and strain tensors and entails a complex linearization involving fourth-order constitutive tensors. In contrast, standard formulations in finite strain continuum mechanics are typically expressed in a fully material framework based on the symmetric second Piola-Kirchhoff (PK2) stress tensor and the right Cauchy-Green or Green-Lagrange (GL) strain tensor [36]. As in linear elasticity, this fully material formulation enables the use of an efficient Voigt matrix-vector representation of symmetric second- and fourth-order tensors, thereby significantly simplifying implementation and reducing computational cost.

Motivated by these advantages, the present work introduces a reformulation of the CSWP for shear-deformable, hyperelastic 3D beams based on a fully material framework in Voigt notation. This approach yields a more concise theoretical description and a computationally more efficient numerical implementation. The highlights of this work are:

1. Energy-conjugate formulation of the CSWP for hyperelastic, shear-deformable 3D beams in terms of PK2 stress and GL strain.
2. Derivation and use of the strain–displacement differential operators (\mathbf{B} and \mathfrak{B}) for solving the CSWP in Voigt notation and for determining the tangent stiffness of the beam.
3. Detailed description of the numerical implementation.

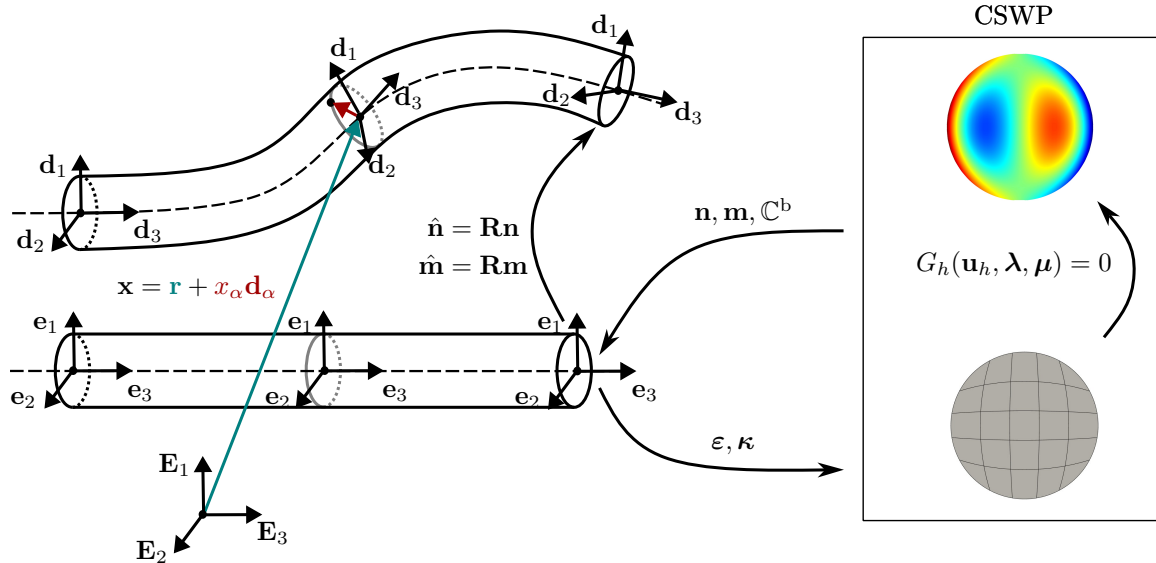


Fig. 1: Deformation map (left) of a geometrically nonlinear beam and schematic representation of the cross-sectional warping problem as a means of obtaining nonlinear constitutive relations suitable for beam theory (right)

4. Numerical verification of the proposed fully material “PK2 formulation” through comparison with a “PK1 formulation” based on [26] and with established results from the literature.
5. Open-source code publication, based on the MATLAB isogeometric analysis library NLIGA [37], at a GitHub repository¹, including all results from both the PK1 and the PK2 formulation.

The remainder of this article is structured as follows: In section 2, a brief introduction to the geometrically exact 3D beam theory is given. This is followed by the derivation of the cross-sectional warping problem in a novel, fully material formulation in section 3. Then, in section 4, an isogeometric finite element discretization of the CSWP is detailed, including the derivation of the \mathbf{B} and \mathfrak{B} strain–displacement operators as well as their use in the determination of the tangent stiffness matrix of the beam. Section 5 provides a detailed verification of the approach, followed by a conclusion in section 6.

¹https://github.com/CPSHub/CSWP_Voigt

Notation: Unless stated otherwise, indices with Roman letters \bullet_i take values $i = 1, 2, 3$, whereas indices with Greek letters \bullet_α take values $\alpha = 1, 2$. Furthermore, in accordance with standard index notation, summation over repeated indices is implied. Partial derivatives are denoted by a comma, such that $\partial_{i\bullet} = \bullet_{,i}$.

2 The geometrically nonlinear beam

2.1 Kinematics

In the geometrically nonlinear beam theory, a shear-deformable beam is defined as a framed curve with centerline $\mathbf{r} : s \mapsto \mathbb{R}^3$, $s \in [0, L]$ being the arc-length coordinate and L the beam length, to which a local orthonormal coordinate system with directors $\mathbf{d}_i(s)$ with $i = 1, 2, 3$ is attached. At each coordinate along the beam centerline, its cross-section is denoted as $\mathcal{A}(s) = \{X_\alpha \mathbf{d}_\alpha(s), (X_1, X_2) \in A\}$, where $A \subset \mathbb{R}^2$ would be $A = \{(X_1, X_2) : |X_1| < a, |X_2| < b\}$ for a beam with rectangular cross-section or $A = \{(X_1, X_2) : X_1^2 + X_2^2 < r^2\}$ for a circular cross-section. The

relationship between \mathbf{d}_i and its reference counterpart \mathbf{D}_i is given by the rotation $\mathbf{R} : s \mapsto \text{SO}(3)$, so that $\mathbf{d}_i(s) = \mathbf{R}(s)\mathbf{D}_i(s)$. Without loss of generality, and in favor of a concise explanation of the theory, only initially straight beams with constant cross-sections are treated here. In that case, $\mathbf{e}_i = \mathbf{D}_i$ and hence $\mathbf{d}_i(s) = \mathbf{R}(s)\mathbf{e}_i(s)$, where \mathbf{e}_i refers to the reference coordinate system. For initially straight beams, it holds that the global coordinate system and the referential coordinate system align, i.e., $\mathbf{e}_i = \mathbf{E}_i$. In general, the kinematic quantities that describe the beam's deformation are $\mathbf{r}(s)$ and $\mathbf{R}(s)$. For a graphic explanation of the beam's configuration and their interplay, see fig. 1 (left).

The deformed configuration $\mathbf{x} \in \mathbb{R}^3$ of the 3D beam continuum is given by

$$\begin{aligned} \mathbf{x}(\mathbf{X}) &= \mathbf{r}(s) + X_\alpha \mathbf{d}_\alpha(s) \\ &= \mathbf{r}(s) + X_\alpha \mathbf{R}(s) \mathbf{e}_\alpha \\ &\quad \forall (X_1, X_2) \in A, \quad s \in [0, L], \end{aligned} \quad (1)$$

where $\mathbf{X} \in \mathbb{R}^3$ refers to the coordinates (X_1, X_2, s) in the reference configuration. The corresponding deformation gradient is

$$\mathbf{F}(\mathbf{X}) = \mathbf{R}((\boldsymbol{\varepsilon} + [\boldsymbol{\kappa}]_\times X_\alpha \mathbf{e}_\alpha) \otimes \mathbf{e}_3 + \mathbf{I}), \quad (2)$$

where $\boldsymbol{\varepsilon}(s) = (\varepsilon_1, \varepsilon_2, \varepsilon_3)^\text{T}$ is the vector of the two shear strains and the axial strain, $\boldsymbol{\kappa}(s) = (\kappa_1, \kappa_2, \kappa_3)^\text{T}$ is the vector of the two curvatures and the twist, and $[\boldsymbol{\kappa}]_\times$ is the skew symmetric cross-product matrix generated by $\boldsymbol{\kappa}$. Explicit dependencies on the arc-length coordinate s have been omitted from eq. (2) for better readability. Note that the strain measures $\boldsymbol{\varepsilon}$ and $\boldsymbol{\kappa}$ uniquely describe the strain state in the beam continuum and are hence referred to in the literature as strain prescriptors [23]. For a thorough derivation of the deformation gradient, we refer to [11, 22]. In terms of \mathbf{r} and \mathbf{R} , the beam strain measures are explicitly expressed as

$$\boldsymbol{\varepsilon} = \mathbf{R}^\text{T} \mathbf{r}' - \mathbf{e}_3, \quad (3)$$

$$\boldsymbol{\kappa} = \text{ax}([\boldsymbol{\kappa}]_\times) = \text{ax}(\mathbf{R}^\text{T} \mathbf{R}'). \quad (4)$$

In eq. (4), the operator $\text{ax}(\bullet)$ extracts the axis of a skew-symmetric matrix and $\partial_s \bullet = \bullet'$ refers to the arc-length derivative.

The deformation gradient in eq. (2) can also be expressed as

$$\mathbf{F} = \mathbf{R} \mathbf{F}^{\{\text{cs}\}}, \quad (5)$$

where $\mathbf{F}^{\{\text{cs}\}}(X_\alpha; \boldsymbol{\varepsilon}(s), \boldsymbol{\kappa}(s))$ can be interpreted as the stretch over the cross-section. However, note that it is not a strict polar decomposition as conventionally used in continuum mechanics, cf. [38], since the strain measures $\boldsymbol{\kappa}, \boldsymbol{\varepsilon}$ still depend on the rotation \mathbf{R} , see eqs. (3) and (4).

2.2 Balance equations

The equilibrium configuration of a beam is governed by the balance equations of linear and angular momenta, given by

$$\hat{\mathbf{n}}' = \mathbf{0}, \quad \forall s \in]0, L[\quad (6)$$

$$\hat{\mathbf{m}}' + \mathbf{r}' \times \hat{\mathbf{n}} = \mathbf{0}, \quad \forall s \in]0, L[\quad (7)$$

where $\hat{\mathbf{n}} = (\hat{n}_1, \hat{n}_2, \hat{n}_3)^\text{T}$ denotes the shear and axial forces, and $\hat{\mathbf{m}} = (\hat{m}_1, \hat{m}_2, \hat{m}_3)^\text{T}$ the bending and torsional moments acting on the deformed beam; see fig. 1. These balance equations can be derived from the equilibrium of an infinitesimal beam segment, see [22] for further details or [11, 32] for a variational derivation.

Note that the balance equations in eqs. (6) and (7) are expressed in the spatial configuration. However, as will be shown throughout this work, constitutive relations are typically formulated in the reference configuration, and the corresponding quantities require a push-forward transformation. For example, the relation between spatial and referential forces and moments is given by

$$\hat{\mathbf{n}} = \mathbf{R} \mathbf{n}, \quad \hat{\mathbf{m}} = \mathbf{R} \mathbf{m}, \quad (8)$$

where $\mathbf{n} = (n_1, n_2, n_3)^\text{T}$ and $\mathbf{m} = (m_1, m_2, m_3)^\text{T}$ denote the forces and moments in the reference configuration, related to their spatial counterparts via the rotation matrix \mathbf{R} . An analogous transformation applies to the strain measures $\boldsymbol{\varepsilon}, \boldsymbol{\kappa}$.

2.3 Constitutive relations

As in 3D continuum mechanics, where strains and stresses are considered to be energetic conjugate pairs associated through an energy potential, a

beam internal energy density potential can also be defined in the beam theory as

$$\Psi^b(\boldsymbol{\varepsilon}, \boldsymbol{\kappa}) = \int_A \Psi(\mathbf{F}(X_\alpha; \boldsymbol{\varepsilon}, \boldsymbol{\kappa})) dA, \quad (9)$$

where $\Psi : \mathbf{F} \mapsto \mathbb{R}$ is a hyperelastic strain energy density function defined per unit volume that depends on the deformation gradient \mathbf{F} over the cross-section. $\Psi^b : (\boldsymbol{\varepsilon}, \boldsymbol{\kappa}) \mapsto \mathbb{R}$ is designated as the beam's energy potential, defined as energy per unit length as it is integrated over the cross-section. Consequently, following [18], the constitutive relations for the beam can be obtained in a thermodynamically consistent manner from the beam potential as

$$\mathbf{n} = \Psi^b_{,\boldsymbol{\varepsilon}}, \quad \mathbf{m} = \Psi^b_{,\boldsymbol{\kappa}}. \quad (10)$$

Analogously, it follows for the beam's stiffness that

$$\mathbb{C}^b_{\boldsymbol{\varepsilon}\boldsymbol{\varepsilon}} = \Psi^b_{, \boldsymbol{\varepsilon}\boldsymbol{\varepsilon}}, \quad \mathbb{C}^b_{\boldsymbol{\kappa}\boldsymbol{\kappa}} = \Psi^b_{, \boldsymbol{\kappa}\boldsymbol{\kappa}}, \quad \mathbb{C}^b_{\boldsymbol{\varepsilon}\boldsymbol{\kappa}} = \Psi^b_{, \boldsymbol{\varepsilon}\boldsymbol{\kappa}}. \quad (11)$$

In linear elasticity theory, which is usually assumed in conventional beam models, the beam potential is assumed to be quadratic in the strain measures, so that

$$\Psi^b = \frac{1}{2} \boldsymbol{\varepsilon}^T \mathbb{C}^b_{\boldsymbol{\varepsilon}\boldsymbol{\varepsilon}} \boldsymbol{\varepsilon} + \frac{1}{2} \boldsymbol{\kappa}^T \mathbb{C}^b_{\boldsymbol{\kappa}\boldsymbol{\kappa}} \boldsymbol{\kappa} + \boldsymbol{\varepsilon}^T \mathbb{C}^b_{\boldsymbol{\varepsilon}\boldsymbol{\kappa}} \boldsymbol{\kappa}, \quad (12)$$

with constant beam stiffness $\mathbb{C}^b_{\boldsymbol{\varepsilon}\boldsymbol{\varepsilon}}$, $\mathbb{C}^b_{\boldsymbol{\varepsilon}\boldsymbol{\kappa}}$, $\mathbb{C}^b_{\boldsymbol{\kappa}\boldsymbol{\kappa}}$. As a consequence, the stress resultants are linear in the strain measures and the constitutive model becomes

$$\begin{pmatrix} \mathbf{n} \\ \mathbf{m} \end{pmatrix} = \begin{pmatrix} \mathbb{C}^b_{\boldsymbol{\varepsilon}\boldsymbol{\varepsilon}} & \mathbb{C}^b_{\boldsymbol{\varepsilon}\boldsymbol{\kappa}} \\ \mathbb{C}^b_{\boldsymbol{\varepsilon}\boldsymbol{\kappa}}^T & \mathbb{C}^b_{\boldsymbol{\kappa}\boldsymbol{\kappa}} \end{pmatrix} \begin{pmatrix} \boldsymbol{\varepsilon} \\ \boldsymbol{\kappa} \end{pmatrix} = \mathbb{C}^b \begin{pmatrix} \boldsymbol{\varepsilon} \\ \boldsymbol{\kappa} \end{pmatrix}. \quad (13)$$

Note that the constitutive model in eq. (13) is linear, does not allow cross-sectional deformation, and is limited to small elastic strains.

3 Cross-sectional warping problem

While simple and widely used, linear constitutive models for 3D beams exhibit clear limitations when large strains and nonlinear material behavior are involved. In practice, cross-sectional deformations occur, and the use of materials beyond

the linear elastic regime is often of interest. However, in this context, it is not appropriate to model hyperelastic behavior in beams by directly evaluating eq. (9) with the deformation gradient given in eq. (2), as this leads to overly stiff responses, see [34].

To account for the influence of general hyperelastic 3D material laws on beam constitutive relations, we follow the approach of Arora et al. [26] and formulate a cross-sectional problem that incorporates both warping and arbitrary hyperelastic material models. As introduced in section 1, this problem is referred to as the cross-sectional warping problem (CSWP) and constitutes the central focus of this work.

3.1 Problem formulation

Cross-sectional warping is introduced by augmenting the deformation map in eq. (1) with the warping function $\mathbf{u} : (s, X_\alpha) \mapsto \mathbb{R}^3$, defined in the reference configuration. The resulting deformation map reads

$$\begin{aligned} \mathbf{x}(\mathbf{X}) &= \mathbf{r}(s) + X_\alpha \mathbf{R}(s) \mathbf{e}_\alpha + u_i(s, X_\alpha) \mathbf{R}(s) \mathbf{e}_i \\ &= \mathbf{r}(s) + \mathbf{x}^{\{\text{cs}\}}, \end{aligned} \quad (14)$$

where $\mathbf{x}^{\{\text{cs}\}}$ denotes the deformation of the cross-section. For the remainder of this manuscript, explicit dependencies on the coordinates \mathbf{X} are omitted for clarity.

Following the procedure introduced in section 2.1, isolating the rotation \mathbf{R} on the left yields

$$\begin{aligned} \mathbf{F} &= \mathbf{R} ((\boldsymbol{\varepsilon} + [\boldsymbol{\kappa}]_\times \mathbf{x}^{\{\text{cs}\}}) \otimes \mathbf{e}_3 + \mathbf{I} + \nabla_\alpha \mathbf{u}) \\ &= \mathbf{R} \mathbf{F}^{\{\text{cs}\}}, \end{aligned} \quad (15)$$

where $\mathbf{F}^{\{\text{cs}\}}$ corresponds to the net deformation gradient of the cross-section, now including the in-plane deformation gradient $\nabla_\alpha \mathbf{u} = \mathbf{u}_{,\alpha} \otimes \mathbf{e}_\alpha$.

In eq. (15), the derivative of the warping function with respect to the arc-length coordinate s is assumed to vanish, i.e., $\mathbf{u}_{,s} = 0$. This assumption enforces a uniform strain field along the beam centerline and reduces the three-dimensional beam problem to its two-dimensional cross-section. Consequently, the deformation gradient \mathbf{F} becomes constant along the beam axis and can, without loss of generality, be evaluated at $s = 0$. At this

location, the assumptions $\mathbf{R} = \mathbf{I}$ and $\mathbf{r}(s=0) = \mathbf{0}$ can be adopted, which yield

$$\begin{aligned} \mathbf{x} \stackrel{\dagger}{=} \mathbf{x}^{\{\text{cs}\}} &= X_\alpha \mathbf{e}_\alpha + u_i(s, X_\alpha) \mathbf{e}_i \\ &= \mathbf{X} + \mathbf{u}, \end{aligned} \quad (16)$$

with $\mathbf{u} : (X_1, X_2) \mapsto \mathbb{R}^3$ and consequently

$$\begin{aligned} \mathbf{F}(X_\alpha, \mathbf{u}(X_\alpha); \boldsymbol{\varepsilon}, \boldsymbol{\kappa}) &\stackrel{\dagger}{=} \mathbf{F}^{\{\text{cs}\}}(s=0) \\ &= (\boldsymbol{\varepsilon} + [\boldsymbol{\kappa}]_\times \mathbf{x}) \otimes \mathbf{e}_3 + \mathbf{I} + \nabla_\alpha \mathbf{u}. \end{aligned} \quad (17)$$

In the following, the deformation gradient is consistently defined as $\mathbf{F} \stackrel{\dagger}{=} \mathbf{F}^{\{\text{cs}\}}$.

In an analogous fashion to eq. (9), the beam internal energy potential can now be expressed as

$$\Psi^b(\boldsymbol{\varepsilon}, \boldsymbol{\kappa}) = \min_{\mathbf{u}} \int_A \psi(\mathbf{F}(X_\alpha, \mathbf{u}(X_\alpha); \boldsymbol{\varepsilon}, \boldsymbol{\kappa})) dA. \quad (18)$$

This means that for given beam strain measures $(\boldsymbol{\varepsilon}, \boldsymbol{\kappa})$, there is a unique warping function \mathbf{u} that minimizes the total strain energy over the cross-section, which is then considered as the beam energy potential Ψ^b . The cross-sectional warping problem thus consists of solving eq. (17) to find \mathbf{u} for given $(\boldsymbol{\varepsilon}, \boldsymbol{\kappa})$. To guarantee an overall unique solution, rigid body motions need to be constrained. For this, as in [23, 26], we use a Lagrange multiplier approach.

3.2 Lagrange multipliers

In order to fix the cross-section in space, the following conditions need to be satisfied

$$\int_A \mathbf{x} dA = \mathbf{0}, \quad \int_A \{\mathbf{x}\}_\times dA = \mathbf{0}, \quad (19)$$

where $\{\mathbf{x}\}_\times$ is defined as

$$\{\mathbf{x}\}_\times = \begin{pmatrix} x_2 x_3 & & \\ x_1 x_3 & & \\ \arctan(\frac{x_2}{x_1}) - \arctan(\frac{X_2}{X_1}) & & \end{pmatrix}. \quad (20)$$

While eq. (19)₁ fixes the cross-section to its center of mass, eq. (19)₂ avoids rotation around its main axes. These conditions are imposed weakly through the Lagrange multipliers $\boldsymbol{\lambda} \in \mathbb{R}^3$ and

$\boldsymbol{\mu} \in \mathbb{R}^3$ and the penalty term

$$\mathcal{L}(\mathbf{u}, \boldsymbol{\lambda}, \boldsymbol{\mu}) = \int_A \boldsymbol{\lambda} \cdot \mathbf{x} + \boldsymbol{\mu} \cdot \{\mathbf{x}\}_\times dA. \quad (21)$$

The following treatment of the Lagrange multiplier method is analogous to the one presented in [32].

3.3 Constrained minimization problem

Combining eqs. (18) and (21), the CSWP can be formulated as a constrained minimization problem for the following functional:

$$\mathcal{F}(\mathbf{u}, \boldsymbol{\lambda}, \boldsymbol{\mu}) = \int_A \psi(\mathbf{F}) + \mathcal{L}(\mathbf{u}, \boldsymbol{\lambda}, \boldsymbol{\mu}) dA. \quad (22)$$

The minimization problem can thus be formulated as: find $\mathbf{u}, \boldsymbol{\mu}, \boldsymbol{\lambda}$ so that the functional \mathcal{F} is minimized.

A stationary solution is obtained by setting the first variation of the functional to zero as

$$G = \delta \mathcal{F} = \int_A \delta \psi + \delta \mathcal{L} dA \stackrel{!}{=} 0, \quad (23)$$

where explicit dependencies have been omitted here for better readability. The terms of this variational, weak form of the CSWP can be expanded into

$$\int_A \delta \psi dA = \int_A \mathbf{S} : \delta \mathbf{E} dA, \quad (24)$$

$$\begin{aligned} \int_A \delta \mathcal{L} dA &= \int_A \mathbf{x} \cdot \delta \boldsymbol{\lambda} + \boldsymbol{\lambda} \cdot \delta \mathbf{u} + \{\mathbf{x}\}_\times \cdot \delta \boldsymbol{\mu} \\ &\quad + (\mathfrak{M} \boldsymbol{\mu}) \cdot \delta \mathbf{u} dA, \end{aligned} \quad (25)$$

with

$$\delta \{\mathbf{x}\}_\times = \mathfrak{M}^T \cdot \delta \mathbf{u} = \begin{pmatrix} 0 & x_3 & x_2 \\ x_3 & 0 & x_1 \\ -\frac{x_2}{x_1^2+x_2^2} & \frac{x_1}{x_1^2+x_2^2} & 0 \end{pmatrix} \delta \mathbf{u}. \quad (26)$$

The problem stated in eq. (23) is nonlinear and its iterative numerical solution using Newton's method requires its linearization

$$\Delta G = \int_A \Delta \delta \psi + \Delta \delta \mathcal{L} dA. \quad (27)$$

Here, it is

$$\Delta\delta\psi = \Delta\mathbf{S} : \delta\mathbf{E} + \mathbf{S} : \Delta\delta\mathbf{E}, \quad (28)$$

$$\begin{aligned} \Delta\delta\mathcal{L} = & \Delta\mathbf{u} \cdot \delta\boldsymbol{\lambda} + \Delta\boldsymbol{\lambda} \cdot \delta\mathbf{u} + \mathfrak{M}^T \cdot \Delta\mathbf{u} \cdot \delta\boldsymbol{\mu} \\ & + \boldsymbol{\Xi} \cdot \Delta\mathbf{u} \cdot \delta\mathbf{u} + \mathfrak{M} \cdot \Delta\boldsymbol{\mu} \cdot \delta\mathbf{u}, \end{aligned} \quad (29)$$

with

$$\boldsymbol{\Xi} = \begin{pmatrix} \mu_3 \frac{2x_1x_2}{(x_1^2+x_2^2)^2} & \mu_3 \frac{x_2^2-x_1^2}{(x_1^2+x_2^2)^2} & \mu_2 \\ \mu_3 \frac{x_2^2-x_1^2}{(x_1^2+x_2^2)^2} & -\mu_3 \frac{2x_1x_2}{(x_1^2+x_2^2)^2} & \mu_1 \\ \mu_2 & \mu_1 & 0 \end{pmatrix} \quad (30)$$

and

$$\delta\mathbf{E} = \frac{1}{2} (\mathbf{F}^T \delta\mathbf{F} + \delta\mathbf{F}^T \mathbf{F}), \quad (31)$$

$$\delta\mathbf{F} = \left(\delta\mathbf{u}_{,1}, \delta\mathbf{u}_{,2}, [\boldsymbol{\kappa}]_{\times} \delta\mathbf{u} \right). \quad (32)$$

In summary, to determine the beam internal energy potential Ψ^b , the variational problem $G = 0$ stated in eq. (23), expressed here in a fully material formulation using the PK2 stress and GL strain tensors, needs to be solved for the warping function \mathbf{u} and the Lagrange multipliers $\boldsymbol{\lambda}, \boldsymbol{\mu}$, using its linearization ΔG provided in eq. (27).

3.4 Stress resultants and beam stiffness

After solving the CSWP and determining the warping function \mathbf{u} for given $(\boldsymbol{\varepsilon}, \boldsymbol{\kappa})$, the stress resultants, i.e., the resultant forces \mathbf{n} and moments \mathbf{m} of the beam theory can be obtained by integrating the traction \mathbf{T} over the reference cross-section:

$$\mathbf{n} = \int_A \mathbf{T} dA \stackrel{\dagger}{=} \Psi_{,\boldsymbol{\varepsilon}}^b, \quad (33)$$

$$\mathbf{m} = \int_A \mathbf{x} \times \mathbf{T} dA \stackrel{\dagger}{=} \Psi_{,\boldsymbol{\kappa}}^b. \quad (34)$$

The traction $\mathbf{T} = \mathbf{P}\mathbf{e}_3$ is defined as the normal projection of the first Piola–Kirchhoff stress tensor \mathbf{P} onto the reference cross-section, where the first and second Piola–Kirchhoff stress tensors are related through $\mathbf{P} = \mathbf{F}\mathbf{S}$. The equivalence between the stress resultants and the derivatives of the implicitly defined potential Ψ^b is further detailed in [26, 32]. Alternatively, eqs. (33) and (34) can be

written in a compact manner as

$$\Psi_{,p}^b = \int_A (\mathbf{P}\mathbf{e}_3) \cdot (\boldsymbol{\varepsilon}_{,p} + [\boldsymbol{\kappa}_{,p}]_{\times} \mathbf{x}) dA, \quad (35)$$

where $p \in \{\varepsilon_1, \varepsilon_2, \varepsilon_3, \kappa_1, \kappa_2, \kappa_3\}$ corresponds to one of the six beam strain measures and thus, e.g., $\boldsymbol{\varepsilon}_{,\varepsilon_1} = (1, 0, 0)^T$. Note that here and in the following, partial derivatives w.r.t. the Cartesian coordinates X_1 and X_2 are denoted by $\bullet_{,1}$ and $\bullet_{,2}$, whereas derivatives with respect to the strain measures are denoted by $\bullet_{,p}$ or $\bullet_{,q}$.

Using the same notation, the coefficients of the beam stiffness matrix $\mathbb{C}^b \in \mathbb{R}^{6 \times 6}$ from eq. (11) are obtained as, see also [23, 26]:

$$\begin{aligned} \mathbb{C}_{pq}^b = & \int_A (\mathbb{A} : \mathbf{F}_{,q}) \mathbf{e}_3 \cdot (\boldsymbol{\varepsilon}_{,p} + [\boldsymbol{\kappa}_{,p}]_{\times} \mathbf{x}) \\ & + (\mathbf{P}\mathbf{e}_3) \cdot ([\boldsymbol{\kappa}_{,p}]_{\times} \mathbf{u}_{,q}) dA \\ \stackrel{\dagger}{=} & \Psi_{,pq}^b \end{aligned} \quad (36)$$

Here, $\mathbb{A} = \frac{\partial \mathbf{P}}{\partial \mathbf{F}} = \frac{\partial^2 \psi}{\partial \mathbf{F}^2}$ corresponds to the tangent stiffness of the constitutive model of the material. Furthermore, the expression $\mathbf{F}_{,q}$ can be expressed explicitly in a column-wise fashion as

$$\mathbf{F}_{,q} = \left(\mathbf{u}_{,q1}, \mathbf{u}_{,q2}, \boldsymbol{\varepsilon}_{,q} + [\boldsymbol{\kappa}_{,q}]_{\times} \mathbf{x} + [\boldsymbol{\kappa}]_{\times} \mathbf{u}_{,q} \right). \quad (37)$$

The actual determination of $\mathbf{u}_{,q}$, the sensitivity of the warping function \mathbf{u} w.r.t. the strain measure q , and its material derivatives $\mathbf{u}_{,q\alpha}$, is non-trivial and will be discussed in section 4.2.

4 Isogeometric finite element discretization

Based on the fully material formulation of the hyperelastic CSWP in terms of the Green–Lagrange strain and second Piola–Kirchhoff stress tensors introduced in eqs. (23) and (27), an efficient isogeometric finite element implementation using the Voigt notation is presented in this section. In addition to determining the warping function \mathbf{u} , the proposed computational framework enables the efficient evaluation of the stress resultants \mathbf{n}, \mathbf{m} , the sensitivities $\mathbf{u}_{,q}$, and consequently also the beam stiffness \mathbb{C}^b . The discretization employs NURBS or B-spline basis

functions and builds upon the isogeometric finite element implementation provided by the open-source library NLIGA [37]. It is emphasized, however, that the proposed formulation of the CSWP in Voigt notation is not restricted to isogeometric analysis and can also be easily implemented within a classical finite element framework.

4.1 Discretization of the CSWP

The discretization of the two-dimensional cross-section and the associated warping function is based on n bivariate B-spline basis functions $N_I(\xi, \eta) : \hat{\Omega} \rightarrow \mathbb{R}$ defined over a parametric domain $\hat{\Omega} \subset \mathbb{R}^2$. For details on the definition of B-spline functions, see for instance [39]. Following the isoparametric concept, the discretized initial and deformed configurations of the cross-section, as well as the warping displacement, are then approximated as

$$\mathbf{X} \approx \mathbf{X}_h(\xi, \eta) = \sum_{I=1}^n N_I(\xi, \eta) \mathbf{X}_I, \quad (38)$$

$$\mathbf{x} \approx \mathbf{x}_h(\xi, \eta) = \mathbf{X}_h(\xi, \eta) + \mathbf{u}_h(\xi, \eta), \quad (39)$$

$$\mathbf{u} \approx \mathbf{u}_h(\xi, \eta) = \sum_{I=1}^n N_I(\xi, \eta) \mathbf{u}_I, \quad (40)$$

where $\mathbf{X}_I \in \mathbb{R}^3$ and $\mathbf{u}_I \in \mathbb{R}^3$ denote the control points associated with the n basis functions. Although the CSWP is defined over a two-dimensional manifold, $\mathbf{X} : \hat{\Omega} \mapsto \mathcal{A}$, each control point possesses three degrees of freedom, thereby allowing for both in-plane and out-of-plane cross-sectional deformations.

Following a standard Galerkin procedure, the corresponding variations of the displacement field and the deformation gradient, see eq. (32), are approximated as

$$\delta \mathbf{u} \approx \delta \mathbf{u}_h(\xi, \eta) = \sum_{I=1}^n N_I(\xi, \eta) \delta \mathbf{u}_I, \quad (41)$$

$$\begin{aligned} \delta \mathbf{F} \approx \delta \mathbf{F}_h(\xi, \eta) &= \sum_{I=1}^n \delta \mathbf{F}_I \\ &= \sum_{I=1}^n \left(N_{I,1} \delta \mathbf{u}_I, N_{I,2} \delta \mathbf{u}_I, N_I [\boldsymbol{\kappa}]_{\times} \delta \mathbf{u}_I \right), \end{aligned} \quad (42)$$

where the material derivatives are obtained via the chain rule and the Jacobian of the geometric

discretization eq. (38) as

$$\nabla N_I = \begin{pmatrix} \partial_1 N_I \\ \partial_2 N_I \end{pmatrix}^T = \begin{pmatrix} \partial_{\xi} N_I \\ \partial_{\eta} N_I \end{pmatrix}^T \begin{pmatrix} \partial_{\xi} X_1 & \partial_{\eta} X_1 \\ \partial_{\xi} X_2 & \partial_{\eta} X_2 \end{pmatrix}^{-1}. \quad (43)$$

Discretized variational form G_h .

These discretizations are now substituted into the variational form given by eq. (23):

$$G_h = G(\mathbf{u}_h, \boldsymbol{\lambda}, \boldsymbol{\mu}) = \int_A \delta \psi_h + \delta \mathcal{L}_h \, dA \stackrel{!}{=} 0. \quad (44)$$

According to eqs. (24) and (25), the individual contributions can be expressed as

$$\int_A \delta \psi_h \, dA = \int_A \sum_{I=1}^n \mathbf{S} : \delta \mathbf{E}_I \, dA, \quad (45)$$

$$\begin{aligned} \int_A \delta \mathcal{L}_h \, dA &= \int_A \mathbf{x}_h \cdot \delta \boldsymbol{\lambda} + \{\mathbf{x}_h\}_{\times} \cdot \delta \boldsymbol{\mu} \\ &\quad + (\mathfrak{M} \boldsymbol{\mu} + \boldsymbol{\lambda}) \cdot \sum_{I=1}^n N_I \delta \mathbf{u}_I \, dA, \end{aligned} \quad (46)$$

where

$$\begin{aligned} \delta \mathbf{E}_I &= \frac{1}{2} (\mathbf{F}^T \delta \mathbf{F}_I + \delta \mathbf{F}_I^T \mathbf{F}) = (\mathbf{F}^T \delta \mathbf{F}_I)^{(s)} \\ &= \left(N_{I,1} \mathbf{F}^T \delta \mathbf{u}_I, N_{I,2} \mathbf{F}^T \delta \mathbf{u}_I, \right. \\ &\quad \left. N_I \mathbf{F}^T [\boldsymbol{\kappa}]_{\times} \delta \mathbf{u}_I \right)^{(s)}. \end{aligned} \quad (47)$$

The superscript $(\bullet)^{(s)} = \frac{1}{2}(\bullet + \bullet^T)$ denotes the symmetric part of $\delta \mathbf{E}_I$. For readability, the discretization index $(\bullet)_h$ is omitted in the following.

Owing to the symmetry of \mathbf{S} and $\delta \mathbf{E}_I$, the integrand in eq. (45) can be rewritten in vector form as

$$\sum_{I=1}^n \mathbf{S} : \delta \mathbf{E}_I = \sum_{I=1}^n \delta \underline{\mathbf{E}}_I^T \underline{\mathbf{S}}, \quad (48)$$

where the Voigt notation is adopted as

$$\begin{aligned} \delta \underline{\mathbf{E}}_I^T &= (\delta E_{11}, \delta E_{22}, \delta E_{33}, 2\delta E_{12}, 2\delta E_{23}, 2\delta E_{13})_I \\ &= (\delta E_1, \delta E_2, E_3, \delta E_4, \delta E_5, \delta E_6)_I, \end{aligned} \quad (49)$$

$$\begin{aligned} \underline{\mathbf{S}}^T &= (S_{11}, S_{22}, S_{33}, S_{12}, S_{23}, S_{13}) \\ &= (S_1, S_2, S_3, S_4, S_5, S_6). \end{aligned} \quad (50)$$

Note that this numbering is consistent with [36] and the implementation in NLIGA [37], although the off-diagonal coefficients are ordered differently in the classical Voigt notation.

Since $\delta \mathbf{E}_I$ is linear in $\delta \mathbf{u}_I$, the relation can be written as

$$\delta \mathbf{E}_I^T = (\mathbf{B}_I \delta \mathbf{u}_I)^T = \delta \mathbf{u}_I^T \mathbf{B}_I^T, \quad (51)$$

where $\mathbf{B}_I^T \in \mathbb{R}^{3 \times 6}$ is the strain–displacement operator, which is obtained as

$$\mathbf{B}_I^T = \begin{pmatrix} \mathbf{F}_1 N_{I,1}, & \mathbf{F}_2 N_{I,2}, & -N_I [\boldsymbol{\kappa}] \times \mathbf{F}_3, \\ \mathbf{F}_1 N_{I,2} + \mathbf{F}_2 N_{I,1}, & \mathbf{F}_3 N_{I,2} - N_I [\boldsymbol{\kappa}] \times \mathbf{F}_2, \\ \mathbf{F}_3 N_{I,1} - N_I [\boldsymbol{\kappa}] \times \mathbf{F}_1 \end{pmatrix}, \quad (52)$$

with the column vectors $\mathbf{F}_i \in \mathbb{R}^3, i = 1, 2, 3$, such that $\mathbf{F} = (\mathbf{F}_1, \mathbf{F}_2, \mathbf{F}_3)$.

Since $G_h = 0$ must hold for any $\delta \mathbf{u}$, $\delta \boldsymbol{\lambda}$, $\delta \boldsymbol{\mu}$ in a minimum $(\mathbf{u}_h, \boldsymbol{\lambda}, \boldsymbol{\mu})$, and thus for any $\delta \mathbf{u}_I$, the following residual vectors must all be zero:

$$\mathbf{f}_I^u = \int_A \mathbf{B}_I^T \mathbf{S} + (\boldsymbol{\lambda} + \boldsymbol{\mathfrak{M}} \cdot \boldsymbol{\mu}) N_I dA \stackrel{!}{=} \mathbf{0}, \quad (53)$$

$$\mathbf{f}^\lambda = \int_A \mathbf{x}_h dA \stackrel{!}{=} \mathbf{0}, \quad (54)$$

$$\mathbf{f}^\mu = \int_A \{\mathbf{x}_h\} \times dA \stackrel{!}{=} \mathbf{0}. \quad (55)$$

Note here that \mathbf{B}_I , \mathbf{S} , $\boldsymbol{\mathfrak{M}}$, and \mathbf{x}_h all depend on \mathbf{u}_h and its coefficients \mathbf{u}_J .

Solution scheme.

Equations (53) to (55) form a $3(n+2)$ -dimensional nonlinear system of equations for the control point displacement vector $\mathbf{U} = (\mathbf{u}_1, \dots, \mathbf{u}_n)$, together with $\boldsymbol{\lambda} \in \mathbb{R}^3$ and $\boldsymbol{\mu} \in \mathbb{R}^3$:

$$\hat{\mathbf{F}}(\hat{\mathbf{U}}) = \mathbf{0}, \quad (56)$$

$$\text{with } \hat{\mathbf{U}} = (\mathbf{U}, \boldsymbol{\lambda}, \boldsymbol{\mu})^T, \quad (57)$$

$$\hat{\mathbf{F}} = (\mathbf{f}^u, \mathbf{f}^\lambda, \mathbf{f}^\mu)^T. \quad (58)$$

Newton’s method is employed to iteratively solve this discretized CSWP, requiring the solution of the linear system

$$\hat{\mathbf{K}}(\hat{\mathbf{U}}_k) \Delta \hat{\mathbf{U}}_k = -\hat{\mathbf{F}}(\hat{\mathbf{U}}_k), \quad (59)$$

in each iteration k . Here,

$$\hat{\mathbf{K}}(\hat{\mathbf{U}}) = \begin{pmatrix} \mathbf{K}^{uu} & \mathbf{K}^{u\lambda} & \mathbf{K}^{u\mu} \\ \mathbf{K}^{\lambda u} & \mathbf{0} & \mathbf{0} \\ \mathbf{K}^{\mu u} & \mathbf{0} & \mathbf{0} \end{pmatrix}, \quad (60)$$

is the tangent stiffness matrix, which will be derived below. Note that $\hat{\mathbf{K}}$ is a symmetric matrix, as $\mathbf{K}^{uu} = \mathbf{K}^{uu^T}$, $\mathbf{K}^{\lambda u} = \mathbf{K}^{u\lambda^T}$, $\mathbf{K}^{\mu u} = \mathbf{K}^{u\mu^T}$, and sparse, as the B-spline basis functions N_I generally have limited, local support.

The solution of eq. (59) is followed by the update step

$$\hat{\mathbf{U}}_{k+1} = \hat{\mathbf{U}}_k + \Delta \hat{\mathbf{U}}_k. \quad (61)$$

For incrementally increasing prescribed $(\boldsymbol{\varepsilon}, \boldsymbol{\kappa})$, the solution at each load step is considered converged once the iteration error falls below a prescribed tolerance.

Tangent stiffness matrix.

For solving the nonlinear system of equations eq. (56), the tangent stiffness matrix is required. Relating to the linearization ΔG in eq. (27), the 3×3 sub-matrices are obtained as:

$$\mathbf{K}_{IJ}^{uu} = \frac{\partial \mathbf{f}_I^u}{\partial \mathbf{u}_J} = \int_A \mathbf{B}_I^T \frac{\partial \mathbf{S}}{\partial \mathbf{E}} \mathbf{B}_J + \mathfrak{B}_{IJ}(\mathbf{S} \otimes \mathbf{I}) + N_I \boldsymbol{\Xi} N_J dA, \quad (62)$$

$$\mathbf{K}_I^{u\lambda} = \frac{\partial \mathbf{f}_I^u}{\partial \boldsymbol{\lambda}} = \int_A N_I \mathbf{I} dA, \quad (63)$$

$$\mathbf{K}_I^{u\mu} = \frac{\partial \mathbf{f}_I^u}{\partial \boldsymbol{\mu}} = \int_A N_I \boldsymbol{\mathfrak{M}} dA, \quad (64)$$

$$\mathbf{K}_J^{\lambda u} = \frac{\partial \mathbf{f}^\lambda}{\partial \mathbf{u}_J} = \int_A N_J \mathbf{I} dA, \quad (65)$$

$$\mathbf{K}_J^{\mu u} = \frac{\partial \mathbf{f}^\mu}{\partial \mathbf{u}_J} = \int_A N_J \boldsymbol{\mathfrak{M}}^T dA. \quad (66)$$

Here, $\mathfrak{B}_{IJ} \in \mathbb{R}^{3 \times 18}$, appearing in the second term of eq. (62), corresponds to a to-be-defined operator and $\mathbf{S} \otimes \mathbf{I} \in \mathbb{R}^{18 \times 3}$ denotes the Kronecker product between \mathbf{S} and the identity tensor $\mathbf{I} \in \mathbb{R}^{3 \times 3}$.

To derive the \mathfrak{B}_{IJ} -operator, we first introduce a column-wise representation of the strain–displacement operator $\mathbf{B}_I^T \in \mathbb{R}^{3 \times 6}$ as

$$\mathbf{B}_I^T = (\mathbf{B}_{1I}, \mathbf{B}_{2I}, \mathbf{B}_{3I}, \mathbf{B}_{4I}, \mathbf{B}_{5I}, \mathbf{B}_{6I}), \quad (67)$$

where the individual components $\underline{\mathbf{B}}_{iI} \in \mathbb{R}^3$, $i = 1, \dots, 6$, are directly obtained from eq. (52). Now, the gradient of $\underline{\mathbf{B}}_{iI}$ w.r.t. the displacement control point \mathbf{u}_J can be expressed as

$$\frac{\partial \underline{\mathbf{B}}_{iI}}{\partial \mathbf{u}_J} = \tilde{\mathfrak{B}}_{iIJ} \in \mathbb{R}^{3 \times 3}. \quad (68)$$

As follows from eq. (52), the operator \mathbf{B}_I depends linearly on \mathbf{F} , which itself is linear in \mathbf{u}_h . Consequently, the computation of $\tilde{\mathfrak{B}}_{iIJ}$ requires the derivatives:

$$\begin{aligned} \frac{\partial \underline{\mathbf{F}}_1}{\partial \mathbf{u}_J} &= N_{J,1} \mathbf{I}, \\ \frac{\partial \underline{\mathbf{F}}_2}{\partial \mathbf{u}_J} &= N_{J,2} \mathbf{I}, \\ \frac{\partial \underline{\mathbf{F}}_3}{\partial \mathbf{u}_J} &= N_J [\boldsymbol{\kappa}]_{\times} \mathbf{I}. \end{aligned} \quad (69)$$

After substituting eq. (69) into eq. (68) and using eq. (52), the following expressions are obtained:

$$\begin{aligned} \tilde{\mathfrak{B}}_{1IJ} &= \frac{\partial \underline{\mathbf{B}}_{1I}}{\partial \mathbf{u}_J} = N_{J,1} N_{I,1} \mathbf{I}, \\ \tilde{\mathfrak{B}}_{2IJ} &= \frac{\partial \underline{\mathbf{B}}_{2I}}{\partial \mathbf{u}_J} = N_{J,2} N_{I,2} \mathbf{I}, \\ \tilde{\mathfrak{B}}_{3IJ} &= \frac{\partial \underline{\mathbf{B}}_{3I}}{\partial \mathbf{u}_J} = -N_J N_I [\boldsymbol{\kappa}]_{\times}^2, \\ \tilde{\mathfrak{B}}_{4IJ} &= \frac{\partial \underline{\mathbf{B}}_{4I}}{\partial \mathbf{u}_J} = (N_{J,2} N_{I,1} + N_{J,1} N_{I,2}) \mathbf{I}, \\ \tilde{\mathfrak{B}}_{5IJ} &= \frac{\partial \underline{\mathbf{B}}_{5I}}{\partial \mathbf{u}_J} = (N_{I,2} N_J - N_{J,2} N_I) [\boldsymbol{\kappa}]_{\times}, \\ \tilde{\mathfrak{B}}_{6IJ} &= \frac{\partial \underline{\mathbf{B}}_{6I}}{\partial \mathbf{u}_J} = (N_{I,1} N_J - N_{J,1} N_I) [\boldsymbol{\kappa}]_{\times}. \end{aligned} \quad (70)$$

From this, the second term in the integral in eq. (62) can be expressed as

$$\sum_{i=1}^6 \frac{\partial \underline{\mathbf{B}}_{iI}}{\partial \mathbf{u}_J} S_i = \sum_{i=1}^6 \tilde{\mathfrak{B}}_{iIJ} S_i = \mathfrak{B}_{IJ} (\underline{\mathbf{S}} \otimes \mathbf{I}), \quad (71)$$

where the components $\tilde{\mathfrak{B}}_{iIJ}$ are assembled into the matrix $\mathfrak{B}_{IJ} \in \mathbb{R}^{3 \times 18}$ as

$$\mathfrak{B}_{IJ} = (\tilde{\mathfrak{B}}_{1IJ}, \tilde{\mathfrak{B}}_{2IJ}, \tilde{\mathfrak{B}}_{3IJ}, \tilde{\mathfrak{B}}_{4IJ}, \tilde{\mathfrak{B}}_{5IJ}, \tilde{\mathfrak{B}}_{6IJ}). \quad (72)$$

4.2 Calculation of the beam stiffness \mathbb{C}^b

As discussed in section 3.4, the sensitivities $\mathbf{u}_{,q}$ of the warping function \mathbf{u} with respect to the strain measures $q \in \{\varepsilon_1, \varepsilon_2, \varepsilon_3, \kappa_1, \kappa_2, \kappa_3\}$ are required for the evaluation of the coefficients \mathbb{C}_{pq}^b of the beam stiffness matrix $\mathbb{C}^b \in \mathbb{R}^{6 \times 6}$, see eq. (36). However, these sensitivities are not directly available from the solution vector $\hat{\mathbf{U}}$ obtained from solving eq. (56).

Typically, deriving the sensitivities $\mathbf{u}_{,q}$ is accompanied by the formulation of an additional weak form and its finite element discretization, which involves complex linearizations and extensive derivations, see [26, 28, 31, 32]. Here, we circumvent this issue by introducing an adjoint equation derived directly from the discretized CSWP.

Derivation of adjoint equation.

To compute the sensitivities, we proceed as in PDE-constrained nonlinear optimization, where the adjoint method is commonly used to obtain the gradient of a function w.r.t. its implicit parameters [40].

So far, we have regarded the strain measures q as fixed parameters in the formulation of the variational form of the CSWP G and its discretized counterpart G_h , see eqs. (23) and (44), from which, the nonlinear system of equations in eq. (56) is derived. Now, if we consider q as variable, the displacement \mathbf{u}_h and its control points \mathbf{u}_I , as well as the Lagrangian multipliers $\boldsymbol{\lambda}, \boldsymbol{\mu}$ are in fact q -dependent through the implicit relations

$$G_h(\mathbf{u}_h(q), \boldsymbol{\lambda}(q), \boldsymbol{\mu}(q)) = 0, \quad (73)$$

$$\Rightarrow \hat{\mathbf{F}}(\hat{\mathbf{U}}(q)) = \mathbf{0}. \quad (74)$$

Directly continuing with the fully discretized nonlinear system of equations, the residual vector $\hat{\mathbf{F}}$ must be stationary w.r.t. q as $\hat{\mathbf{U}}(q)$ is always determined such that eq. (74) is satisfied. Hence, it follows that

$$\begin{aligned} \frac{d\hat{\mathbf{F}}}{dq} &\stackrel{!}{=} \mathbf{0}, \\ \Leftrightarrow \frac{\partial \hat{\mathbf{F}}}{\partial \hat{\mathbf{U}}} \cdot \frac{\partial \hat{\mathbf{U}}}{\partial q} + \frac{\partial \hat{\mathbf{F}}}{\partial q} &= \mathbf{0}, \\ \Leftrightarrow \hat{\mathbf{K}} \hat{\mathbf{Y}} &= -\hat{\mathbf{F}}_{,q}. \end{aligned} \quad (75)$$

where $\hat{\mathbf{K}}$ denotes the tangent stiffness matrix from eq. (60). The unknowns of the linear system in eq. (75) are $\hat{\mathbf{Y}} = (\mathbf{U}_q, \boldsymbol{\lambda}_q, \boldsymbol{\mu}_q)$, which comprise the vector of displacement control point sensitivities $\mathbf{U}_q = (\mathbf{u}_{1,q}, \dots, \mathbf{u}_{n,q})$ as well as the sensitivities of the Lagrange multipliers with respect to q , i.e., $\boldsymbol{\lambda}_q$ and $\boldsymbol{\mu}_q$. $\hat{\mathbf{F}}_{,q}$ describes the sensitivities of the residual vector, which are derived below.

After solving the linear system of eq. (75), for which $\hat{\mathbf{K}}$ can be used directly from the last Newton iteration with the converged $\hat{\mathbf{U}}$, the sensitivity \mathbf{u}_q and its derivatives with respect to the coordinates X_α can be obtained directly from the finite element interpolation of eq. (40):

$$\mathbf{u}_q = \sum_{I=1}^n N_I \mathbf{u}_{I,q}, \quad \mathbf{u}_{q\alpha} = \sum_{I=1}^n N_{I,\alpha} \mathbf{u}_{I,q}. \quad (76)$$

In total, the computation of the beam stiffness \mathbb{C}_{pq}^b requires six sensitivities, each corresponding to one strain measure $q \in \{\varepsilon_1, \varepsilon_2, \varepsilon_3, \kappa_1, \kappa_2, \kappa_3\}$, see eq. (36). The overall procedure is summarized in algorithm 1.

Algorithm 1 Beam stiffness matrix \mathbb{C}^b

Require: $\hat{\mathbf{K}}$ from eq. (59)

- 1: $q = (\varepsilon_1, \varepsilon_2, \varepsilon_3, \kappa_1, \kappa_2, \kappa_3)^T$
 - 2: **for** $j = 1$ to 6 **do**
 - 3: Evaluate $\hat{\mathbf{F}}_{,q}(q_j)$ from eqs. (77) to (79)
 - 4: Solve $\hat{\mathbf{K}}\hat{\mathbf{Y}} = -\hat{\mathbf{F}}_{,q}$
 - 5: $\hat{\mathbf{U}}_q \leftarrow \hat{\mathbf{Y}}$
 - 6: **for** $i = 1$ to 6 **do**
 - 7: \mathbb{C}_{ij}^b from eq. (36) using eq. (76)
 - 8: **end for**
 - 9: **end for**
-

Sensitivities of the residual vector.

For solving eq. (75), the derivation and evaluation of the sensitivities of the residual vector $\hat{\mathbf{F}}_{,q}$ is required. Accordingly, taking the partial derivative of eqs. (53) to (55) with respect to the strain measure q yields

$$\mathbf{f}_{I,q}^u = \int_A \mathbf{B}_I^T 2 \frac{\partial \underline{\mathbf{S}}}{\partial \underline{\mathbf{C}}} \mathbf{E}_{,q} + \mathbf{B}_{I,q}^T \underline{\mathbf{S}} dA \quad (77)$$

$$\mathbf{f}_{,q}^\lambda = \int_A \mathbf{0} dA, \quad (78)$$

$$\mathbf{f}_{,q}^\mu = \int_A \mathbf{0} dA \quad (79)$$

To derive $\underline{\mathbf{E}}_{,q}$, appearing in the first term of eq. (77), we first consider its tensorial form

$$\mathbf{E}_{,q} = \frac{1}{2} (\mathbf{F}_{,q}^T \mathbf{F} + \mathbf{F}^T \mathbf{F}_{,q}) = (\mathbf{F}^T \mathbf{F}_{,q})^{(s)}, \quad (80)$$

where it follows from eq. (17) that

$$\mathbf{F}_{,q} = (\mathbf{0}, \mathbf{0}, \boldsymbol{\varepsilon}_{,q} + [\boldsymbol{\kappa}_{,q}] \times \mathbf{x}). \quad (81)$$

In Voigt notation, eq. (80) can be expressed as

$$\underline{\mathbf{E}}_{,q} = (0, 0, E_{3,q}, 0, E_{5,q}, E_{6,q})^T, \quad (82)$$

where

$$\begin{aligned} E_{3,q} &= \underline{\mathbf{F}}_3^T (\boldsymbol{\varepsilon}_{,q} + [\boldsymbol{\kappa}_{,q}] \times \mathbf{x}), \\ E_{5,q} &= \underline{\mathbf{F}}_2^T (\boldsymbol{\varepsilon}_{,q} + [\boldsymbol{\kappa}_{,q}] \times \mathbf{x}), \\ E_{6,q} &= \underline{\mathbf{F}}_1^T (\boldsymbol{\varepsilon}_{,q} + [\boldsymbol{\kappa}_{,q}] \times \mathbf{x}). \end{aligned} \quad (83)$$

Furthermore, to determine $\mathbf{B}_{I,q}^T$, appearing in the second term of eq. (77), we recall the definition of the \mathbf{B}_I^T -operator in eq. (52). Its partial derivative w.r.t the strain measure q leads to

$$\begin{aligned} \mathbf{B}_{I,q}^T &= (\underline{\mathbf{B}}_{1I,q}, \underline{\mathbf{B}}_{2I,q}, \underline{\mathbf{B}}_{3I,q}, \underline{\mathbf{B}}_{4I,q}, \underline{\mathbf{B}}_{5I,q}, \underline{\mathbf{B}}_{6I,q}) \\ &= (\mathbf{0}, \mathbf{0}, \underline{\mathbf{B}}_{3I,q}, \mathbf{0}, \underline{\mathbf{B}}_{5I,q}, \underline{\mathbf{B}}_{6I,q}), \end{aligned} \quad (84)$$

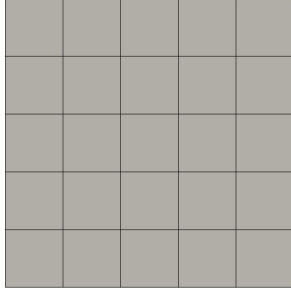
where

$$\begin{aligned} \underline{\mathbf{B}}_{3I,q} &= -N_I ([\boldsymbol{\kappa}_{,q}] \times \underline{\mathbf{F}}_3 + [\boldsymbol{\kappa}] \times (\boldsymbol{\varepsilon}_{,q} + [\boldsymbol{\kappa}_{,q}] \times \mathbf{x})), \\ \underline{\mathbf{B}}_{5I,q} &= N_{I,2} (\boldsymbol{\varepsilon}_{,q} + [\boldsymbol{\kappa}_{,q}] \times \mathbf{x}) - N_I [\boldsymbol{\kappa}_{,q}] \times \underline{\mathbf{F}}_2, \\ \underline{\mathbf{B}}_{6I,q} &= N_{I,1} (\boldsymbol{\varepsilon}_{,q} + [\boldsymbol{\kappa}_{,q}] \times \mathbf{x}) - N_I [\boldsymbol{\kappa}_{,q}] \times \underline{\mathbf{F}}_1. \end{aligned} \quad (85)$$

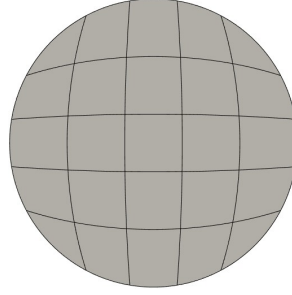
5 Results

In this section, the present fully material, PK2 formulation of the CSWP is compared against results found in literature and against the analogous PK1 formulation from [26, 32]. The solution \mathbf{u} of the CSWP, as well as subsequent post-processed quantities, the beam stress resultants \mathbf{n}, \mathbf{m} and stiffness \mathbb{C}^b , are compared and discussed.

For the results presented here, and without loss of generality, use of two exemplary cross-sections



(a) Isogeometric mesh of unit square cross-section.



(b) Isogeometric mesh of unit circle cross-section.

Fig. 2: Exemplary meshes for the two cross-sections: (a) square and (b) circle.

is made: a unit square of side length 1.0 mm and a unit circle of radius 1.0 mm. These are both parametrized using B-Splines as follows with 5 elements (knot spans) and degree $p = 3$ in both parametric directions, see fig. 2. Thus, there is a total of $n = 64 = (3 + 5)^2$ shape functions and control points for the discretization of the warping displacement, see eq. (40).

Three different common hyperelastic material models are used for the constitutive relation, all available in the open source library NLIGA [37]: Saint Venant-Kirchhoff (SVK), Neo-Hooke (NH), and Mooney-Rivlin (MR). Relevant parameters, strain energy density formulations and modeling coefficients for the NH and MR approaches can be found within table 1.

For validation purposes, the PK1 formulation presented in [32] was also implemented using NLIGA and was further used here as a means of comparison for the newly proposed formulation. Consequently, a thorough comparison between both formulations is made, yielding exactly the same results – as shown in the following.

In this section, for simplicity, the formulation from [26, 32] is denoted as the “PK1 formulation”, while the proposed fully material formulation in Voigt notation is denoted as the “PK2 formulation”.

Comparison of residuals.

A first indicator that both formulations are equivalent is the fact that they yield the same stiffness matrix $\hat{\mathbf{K}}$ and, consequently, the L^2 -norm of the residual vector $\hat{\mathbf{F}}$ remains the same for both formulations in every Newton iteration, see table 2 for an example with $\boldsymbol{\varepsilon} = (0.02, 0.03, 0.1)$, $\boldsymbol{\kappa} =$

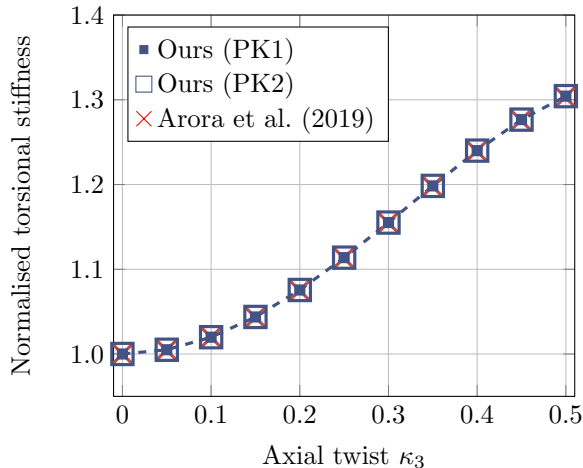
Table 1: Relevant strain energy density formulations and material parameters.

Strain energy density formulations			
\bar{I}_1, \bar{I}_2	: First and second isochoric invariants of \mathbf{C}		
J	: Jacobian determinant of \mathbf{F}		
$\Psi_{\text{SVK}}(\mathbf{C})$	$= \frac{\lambda}{8}(\text{tr}(\mathbf{C} - \mathbf{I}))^2 + \frac{\mu}{4}\text{tr}((\mathbf{C} - \mathbf{I})^2)$		
$\Psi_{\text{NH}}(\mathbf{C})$	$= A_{10}(\bar{I}_1 - 3) + \frac{K}{2}(J - 1)^2$		
$\Psi_{\text{MR}}(\mathbf{C})$	$= B_{10}(\bar{I}_1 - 3) + B_{01}(\bar{I}_2 - 3) + \frac{K}{2}(J - 1)^2$		
Variable	Material parameter	Value	Unit
λ	1st Lamé parameter	121	GPa
μ	2nd Lamé parameter	80	GPa
ν	Poisson’s ratio	0.3	–
E	Young’s modulus	208.16	GPa
K	Bulk modulus	174.34	GPa
A_{10}	NH coefficient ($\frac{\mu}{2}$)	40	GPa
B_{10}	MR coefficient 1 ($0.75 \cdot \frac{\mu}{2}$)	30	GPa
B_{01}	MR coefficient 2 ($0.25 \cdot \frac{\mu}{2}$)	10	GPa

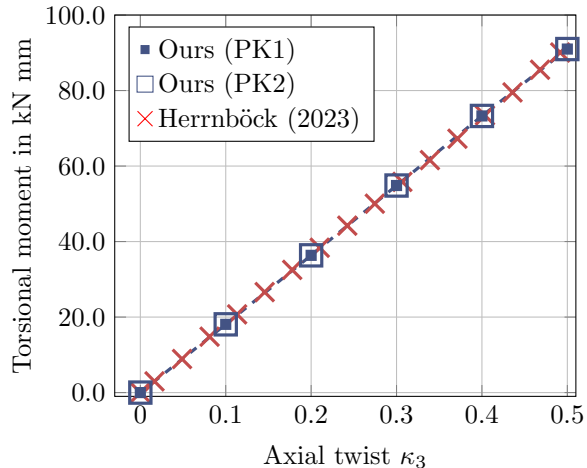
$(0.01, 0.02, 0.02)$, applied to the unit square cross-section using the presented SVK material.

Pure torsion behavior.

For validation of the implementation, a beam cross-section’s reaction to torsion is compared to results found in the literature. Following [26], a rectangular cross-section with aspect ratio $a/b = 2$ is modeled using a SVK material with $\lambda = 1.275$, $\mu = 1.0$. The dependency of the torsional stiffness on a prescribed axial twist κ_3 is compared to data from [26], see fig. 3. The normalized torsional stiffnesses in the present formulations exactly match the results from literature. Furthermore, a unit-square beam cross-section with SVK material and



(a) Comparison of torsional stiffness against literature [26] for a rectangular cross-section



(b) Comparison of torsional moment against literature [32] for a square cross-section

Fig. 3: Validation of torsional responses against literature references.

Table 2: L^2 -norm of the residual vectors for PK1 and PK2 formulations in an exemplary loading with $\varepsilon = (0.02, 0.03, 0.1)$, $\kappa = (0.01, 0.02, 0.02)$.

Newton step k	Residual (PK1)	Residual (PK2)
1	-	-
2	2.61×10^{-1}	2.61×10^{-1}
3	5.20×10^{-6}	5.20×10^{-6}
4	2.37×10^{-14}	2.37×10^{-14}

Lamé parameters $\lambda = 109995,8$ MPa and $\mu = 80194$ MPa from [32] is investigated. Here, the torsional moment m_3 over the axial twist κ_3 is evaluated against results presented in [32]. Again, the results match exactly with the reference.

Multi-axial loading behavior.

For a multi-axial loading case dominated by axial strain with $\varepsilon = (0.02, 0.03, 0.1)$, $\kappa = (0.01, 0.02, 0.02)$, the warping displacement \mathbf{u} is computed on the presented unit square and unit circle cross-sections using both PK1 and PK2 formulations with the SVK material. A color-gradient representation of the out-of-plane component u_3 is shown in fig. 4, highlighting the identical nature of the solution.

Post-processing quantities for the unit-square cross-section are also compared between both formulations. A linear scaling of the previously presented multi-axial loading case using the load scaling factor $\theta \in [0, 1]$ is employed, where $\theta = 0$ is no strain and $\theta = 1$ represents full loading. For each load step, the normal force and axial stiffness are compared between PK1 and PK2 formulations in fig. 5 for all three material models described in table 1. Again, it is visible that both PK1 and PK2 formulations match exactly, independent of the material model.

Pure shear behavior.

For a more visual analysis, a uniaxial pure shear load is investigated in fig. 6 for the unit square and unit circle cross-sections with the SVK material presented in table 1. Here, the out-of-plane displacement and the von Mises equivalent stress are visualized. We report that the out-of-plane deformation matches qualitatively the examples found in the literature [26, 32]. Note that the circular cross-section exhibits a stress singularity in the von Mises stress, which is not displayed in fig. 6. This, however, is traced back to the singular isogeometric parametrization of a circle and not an issue related to the CSWP itself. Additional interactive visualizations of the results can be found in the corresponding [GitHub repository](#).

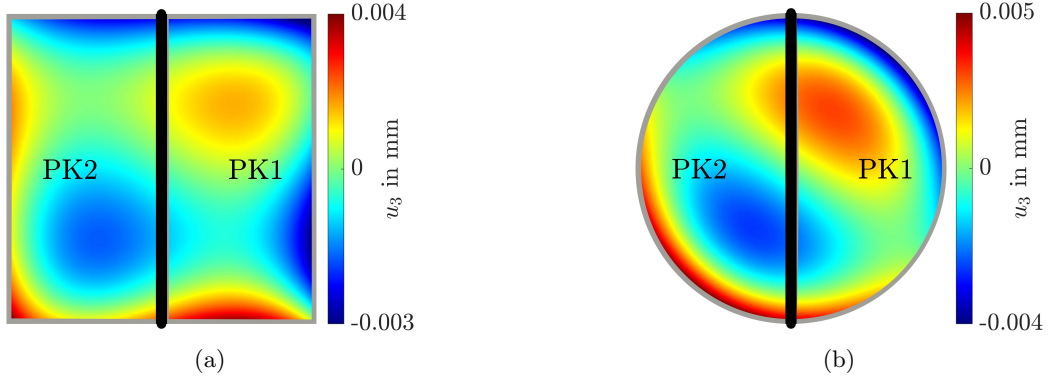


Fig. 4: Distribution of out-of-plane displacement u_3 for (a) a square and (b) a circular cross-section under a multi-axial, stretch-dominated loading state. Solutions derived using the PK1 and PK2 formulations are separated by a black vertical line. The gray background indicates the undeformed cross-sections.

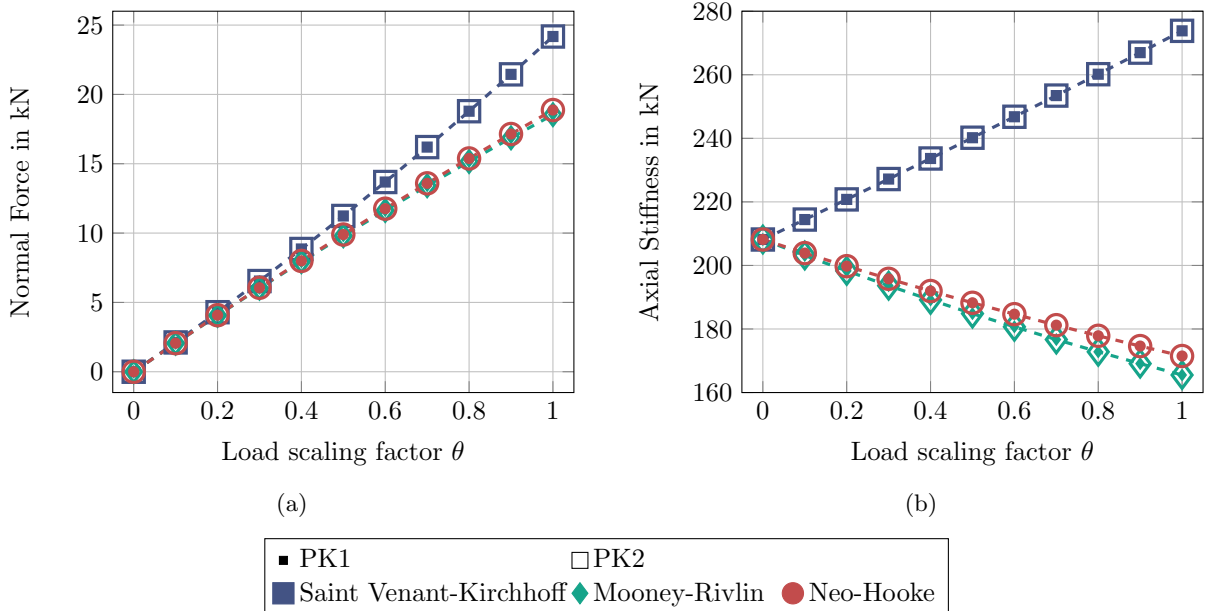


Fig. 5: Comparison of responses for the different material models for (a) normal force and (b) axial stiffness as a function of the load scaling factor θ for the applied multi-axial, stretch-dominated loading on the unit-square cross-section.

6 Conclusion

In this contribution, we reinterpret the cross-sectional warping problem for hyperelastic beams and propose a fully material formulation based on the PK2 stress and GL strain tensors. The proposed formulation exploits their symmetric structure, enabling the use of Voigt notation and thereby reducing fourth-order elasticity tensors

and second-order stress tensors to a matrix-vector representation. This leads, by design, to improved computational efficiency. To formulate the CSWP in Voigt notation, the classical \mathbf{B} - and \mathfrak{B} -operators of nonlinear FEM are modified to exactly represent the cross-sectional deformation and its associated deformation gradient in terms of the strain measures of the beam theory.

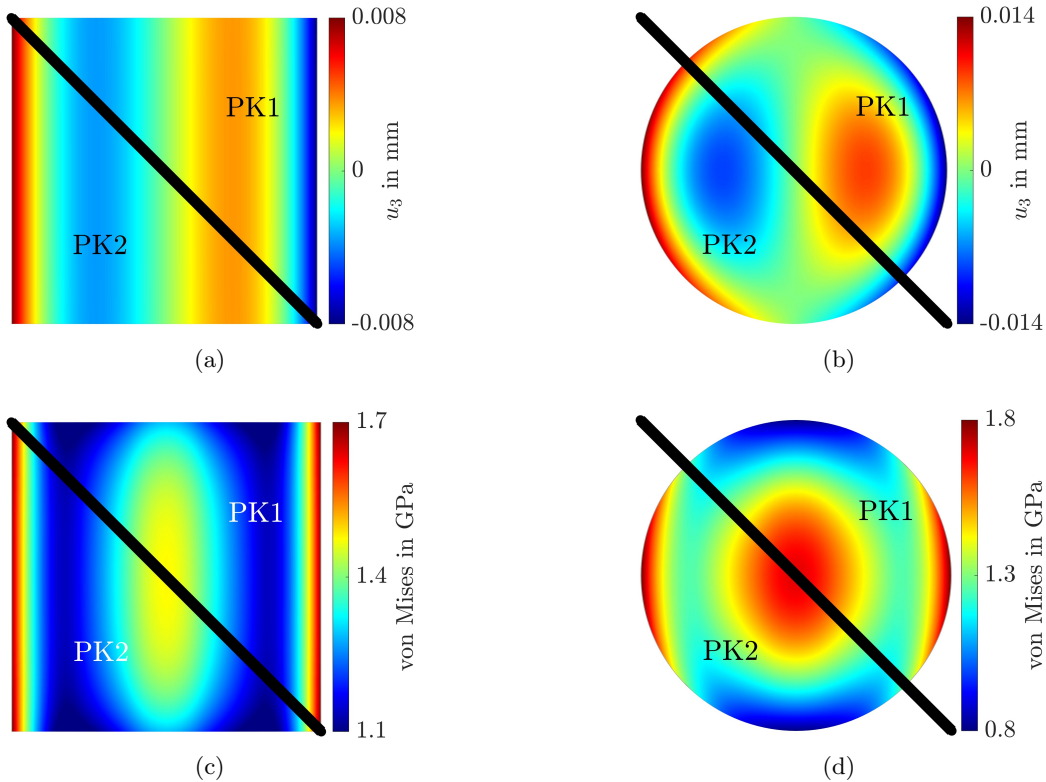


Fig. 6: Comparison between the distributions of out-of-plane Displacement u_3 (a, b) and the associated von Mises stresses (c, d) for a square and a circular cross-section under pure shear ($\varepsilon = [0.1, 0, 0]$). Solutions derived using the PK1 and PK2 formulations are separated by a black diagonal.

The proposed formulation is verified by reproducing results available in the literature. In addition, we implement the corresponding PK1 formulation of [26, 32] and compare both approaches under multi-axial loading. The resulting forces, moments, stiffnesses, and iteration errors are found to be identical in both formulations.

To promote reproducibility, the implementations of both formulations, together with all numerical results, are made available in a [GitHub repository](#). This may serve to promote broader adoption and further extension of the proposed formulation to related problems involving nonlinear beam constitutive models.

Owing to its close connection to classical nonlinear finite element formulations, the present approach can be naturally extended to more complex settings, such as plasticity [41] and multiphysics problems, e.g., chemoelasticity [42]. For geometrically complex cross-sections, further gains in computational efficiency may be achieved,

for instance, by formulating the CSWP as an immersed problem, as demonstrated by Elbadry et al. [43] within a general 2D hyperelasticity framework using NLIGA.

Supplementary information. An accompanying [GitHub repository](#) contains all numerical results and implementations presented in this work, enabling full reproducibility and providing access to the capabilities described in the paper.

Acknowledgements. The authors acknowledge the financial support provided by the Deutsche Forschungsgemeinschaft (DFG, German Research Foundation, project number 460684687), as well as the Graduate School of Computational Engineering at TU Darmstadt.

References

- [1] Priestley, M.J.N., Kowalsky, M.J.: Direct displacement-based seismic design of concrete

- buildings. *Bulletin of the New Zealand Society for Earthquake Engineering* **33**(4), 421–444 (2000) <https://doi.org/10.5459/bnzsee.33.4.421-444>
- [2] Rus, D., Tolley, M.T.: Design, fabrication and control of soft robots. *Nature* **521**(7553), 467–475 (2015) <https://doi.org/10.1038/nature14543>
- [3] Burgner-Kahrs, J., Rucker, D.C., Choset, H.: Continuum robots for medical applications: A survey. *IEEE Transactions on Robotics* **31**(6), 1261–1280 (2015) <https://doi.org/10.1109/TRO.2015.2489500>
- [4] Xia, X., Afshar, A., Yang, H., Portela, C.M., Kochmann, D.M., Di Leo, C.V., Greer, J.R.: Electrochemically reconfigurable architected materials. *Nature* **573**(7773), 205–213 (2019) <https://doi.org/10.1038/s41586-019-1538-z>
- [5] Janbaz, S., Narooei, K., Van Manen, T., Zadpoor, A.: Strain rate-dependent mechanical metamaterials. *Science advances* **6**(25), 0616 (2020) <https://doi.org/10.1126/sciadv.aba0616>
- [6] Karthikeyan, V., Surjadi, J.U., Li, X., Fan, R., Theja, V.C.S., Li, W.J., Lu, Y., Roy, V.A.L.: Three dimensional architected thermoelectric devices with high toughness and power conversion efficiency. *Nature Communications* **14**(1), 2069 (2023) <https://doi.org/10.1038/s41467-023-37707-2>
- [7] Weeger, O., Valizadeh, I., Mistry, Y., Bhate, D.: Inelastic finite deformation beam modeling, simulation, and validation of additively manufactured lattice structures. *Additive Manufacturing Letters* **4**, 100111 <https://doi.org/10.1016/j.addlet.2022.100111>
- [8] Weeger, O., Sakhaei, A.H., Tan, Y.Y., Quek, Y.H., Lee, T.L., Yeung, S.-K., Kaijima, S., Dunn, M.L.: Nonlinear multi-scale modelling, simulation and validation of 3D knitted textiles. *Applied Composite Materials* **25**(4), 797–810 (2018) <https://doi.org/10.1007/s10443-018-9702-4>
- [9] Ding, Z., Weeger, O., Qi, H.J., Dunn, M.L.: 4D Rods: 3D Structures via Programmable 1D Composite Rods. *Materials & Design* **137**, 256–265 <https://doi.org/10.1016/j.matdes.2017.10.004>
- [10] Antman, S.S.: *Nonlinear Problems of Elasticity*, 2nd edn. *Applied Mathematical Sciences*, vol. 107. Springer, NY (2005). <https://doi.org/10.1007/0-387-27649-1>
- [11] Auricchio, F., Carotenuto, P., Reali, A.: On the geometrically exact beam model: A consistent, effective and simple derivation from three-dimensional finite-elasticity. *International Journal of Solids and Structures* **45**(17), 4766–4781 (2008) <https://doi.org/10.1016/j.ijsolstr.2008.04.015>
- [12] Eugster, S.R.: On the foundations of continuum mechanics and its application to beam theories. PhD thesis, ETH Zurich (2014). <https://doi.org/10.3929/ethz-a-010255287>
- [13] Meier, C., Popp, A., Wall, W.A.: Geometrically Exact Finite Element Formulations for Slender Beams: Kirchhoff–Love Theory Versus Simo–Reissner Theory. *Archives of Computational Methods in Engineering* **26**(1), 163–243 (2019) <https://doi.org/10.1007/s11831-017-9232-5>
- [14] Mittelstedt, C.: *Structural Mechanics in Lightweight Engineering*. Springer, Cham (2021). <https://doi.org/10.1007/978-3-030-75193-7>
- [15] Choi, M.-J., Sauer, R.A., Klinkel, S.: An isogeometric finite element formulation for geometrically exact Timoshenko beams with extensible directors. *Computer Methods in Applied Mechanics and Engineering* **385**, 113993 (2021) <https://doi.org/10.1016/j.cma.2021.113993>
- [16] Ignesti, D., Ferri, G., Reali, A., Auricchio, F., Kiendl, J., Marino, E.: A novel finite-strain mixed isogeometric collocation formulation for hyperelastic geometrically exact beams. *Computer Methods in Applied Mechanics and Engineering* **450**, 118641 (2026) <https://doi.org/10.1016/j.cma.2025.118641>

- [17] Smriti, Kumar, A., Steinmann, P.: A finite element formulation for a direct approach to elastoplasticity in special Cosserat rods. *International Journal for Numerical Methods in Engineering* **122**(5), 1262–1282 (2021) <https://doi.org/10.1002/nme.6566>
- [18] Smriti, Kumar, A., Großmann, A., Steinmann, P.: A thermoelastoplastic theory for special Cosserat rods. *Mathematics and Mechanics of Solids* **24**(3), 686–700 (2019) <https://doi.org/10.1177/1081286517754132>
- [19] Weeger, O., Schillinger, D., Müller, R.: Mixed isogeometric collocation for geometrically exact 3D beams with elasto-visco-plastic material behavior and softening effects. *Computer Methods in Applied Mechanics and Engineering* **399**, 115456 (2022) <https://doi.org/10.1016/j.cma.2022.115456>
- [20] Ferri, G., Ignesti, D., Marino, E.: An efficient displacement-based isogeometric formulation for geometrically exact viscoelastic beams. *Computer Methods in Applied Mechanics and Engineering* **417**, 116413 (2023) <https://doi.org/10.1016/j.cma.2023.116413>
- [21] Parida, A., Gupta, P.: A variationally consistent chemo-elastic theory for special cosserat rods. *International Journal of Solids and Structures* **331**, 113912 (2026) <https://doi.org/10.1016/j.ijsolstr.2026.113912>
- [22] Alzate Cobo, J.C., Peng, X.-L., Xu, B.-X., Weeger, O.: A finite swelling 3D beam model with axial and radial diffusion. *Computer Methods in Applied Mechanics and Engineering* **441**, 117983 (2025) <https://doi.org/10.1016/j.cma.2025.117983>
- [23] Herrnböck, L., Kumar, A., Steinmann, P.: Geometrically exact elastoplastic rods: determination of yield surface in terms of stress resultants. *Computational Mechanics* **67**(3), 723–742 (2021) <https://doi.org/10.1007/s00466-020-01957-4>
- [24] Herrnböck, L., Kumar, A., Steinmann, P.: Two-scale off-and online approaches to geometrically exact elastoplastic rods. *Computational Mechanics* **71**(1), 1–24 (2023) <https://doi.org/10.1007/s00466-022-02204-8>
- [25] Gärtner, T., Boom, S., Weerheijm, J., Sluys, L.: A strategy for scaling the hardening behavior in finite element modelling of geometrically exact beams. *Computational Mechanics* **75**(5), 1471–1482 (2025) <https://doi.org/10.1007/s00466-024-02572-3>
- [26] Arora, A., Kumar, A., Steinmann, P.: A computational approach to obtain nonlinearly elastic constitutive relations of special Cosserat rods. *Computer Methods in Applied Mechanics and Engineering* **350**, 295–314 (2019) <https://doi.org/10.1016/j.cma.2019.02.032>
- [27] Kumar, A., Kumar, S., Gupta, P.: A Helical Cauchy-Born Rule for Special Cosserat Rod Modeling of Nano and Continuum Rods. *Journal of Elasticity* **124**(1), 81–106 (2016) <https://doi.org/10.1007/s10659-015-9562-1>
- [28] Singh, R., Arora, A., Kumar, A.: A computational framework to obtain nonlinearly elastic constitutive relations of special Cosserat rods with surface energy. *Computer Methods in Applied Mechanics and Engineering* **398**, 115256 (2022) <https://doi.org/10.1016/j.cma.2022.115256>
- [29] Vinayak, Smriti, Kumar, A.: Uniformly strained anisotropic elastoplastic rods: Determination of elastoplastic constitutive relations and yield surface in terms of rod's variables. *European Journal of Mechanics - A/Solids* **98**, 104867 (2023) <https://doi.org/10.1016/j.euromechsol.2022.104867>
- [30] Kumar, R., Agarwal, V., Kumar, A.: A computational approach to obtain nonlinearly elastic constitutive relations of strips modeled as a special Cosserat rod. *Computer Methods in Applied Mechanics and Engineering* **418**, 116553 (2024) <https://doi.org/10.1016/j.cma.2023.116553>
- [31] Kumar, R., Kumar, A.: Growth-modulated natural shape and stiffnesses of elastic rods modeled as a special Cosserat rod. *European Journal of Mechanics - A/Solids* **116**, 105943 (2026) <https://doi.org/10.1016/j.euromechsol.2026.105943>

- [32] Herrnböck, L.: Numerische Methoden zur Modellierung elastoplastischer Balken und ihre Anwendung auf periodische Gitterstrukturen. PhD thesis, Friedrich-Alexander-Universität Erlangen-Nürnberg (2023)
- [33] Le Clézio, H., Lestringant, C., Kochmann, D.M.: A numerical two-scale approach for nonlinear hyperelastic beams and beam networks. *International Journal of Solids and Structures* **276**, 112307 (2023) <https://doi.org/10.1016/j.ijsolstr.2023.112307>
- [34] Schommartz, J.O., Klein, D.K., Alzate Cobo, J.C., Weeger, O.: Physics-augmented neural networks for constitutive modeling of hyperelastic geometrically exact beams. *Computer Methods in Applied Mechanics and Engineering* **435**, 117592 (2025) <https://doi.org/10.1016/j.cma.2024.117592>
- [35] Le Clézio, H., Karapiperis, K., Kochmann, D.M.: Nonlinear two-scale beam simulations accelerated by thermodynamics-informed neural networks. *Extreme Mechanics Letters* **73**, 102260 (2024) <https://doi.org/10.1016/j.eml.2024.102260>
- [36] Wriggers, P.: *Nonlinear Finite Element Methods*, 1st edn. Springer, Heidelberg (2008). <https://doi.org/10.1007/978-3-540-71001-1>
- [37] Du, X., Zhao, G., Wang, W., Guo, M., Zhang, R., Yang, J.: NLIGA: A MATLAB framework for nonlinear isogeometric analysis. *Computer Aided Geometric Design* **80**, 101869 (2020) <https://doi.org/10.1016/j.cagd.2020.101869>
- [38] Holzapfel, G.A.: *Nonlinear Solid Mechanics: A Continuum Approach for Engineering*. Wiley, Chichester Weinheim (2010)
- [39] Piegl, L., Tiller, W.: *The NURBS Book*, 2nd edn. Springer, Heidelberg (1997). <https://doi.org/10.1007/978-3-642-59223-2>
- [40] Hinze, M., Pinnau, R., Ulbrich, M., Ulbrich, S.: *Optimization with PDE Constraints*. Mathematical Modelling: Theory and Applications, vol. 23. Springer. <https://doi.org/10.1007/978-1-4020-8839-1>
- [41] Eidel, B., Gruttmann, F.: Elastoplastic orthotropy at finite strains: multiplicative formulation and numerical implementation. *Computational Materials Science* **28**(3-4), 732–742 (2003) <https://doi.org/10.1016/j.commatsci.2003.08.027>
- [42] Shafqat, A., Weeger, O., Xu, B.-X.: A robust finite strain isogeometric chemomechanics solid-beam element. *Computer Methods in Applied Mechanics and Engineering* **448**, 118457 (2025) <https://doi.org/10.1016/j.cma.2025.118457>
- [43] Elbadry, Y.T., Antolín, P., Weeger, O.: Immersed isogeometric analysis with boundary conformal quadrature for finite deformation elasticity. *Archive of Applied Mechanics* **95**(9), 219 (2025) <https://doi.org/10.1007/s00419-025-02924-2>